A comparative molecular field analysis study of obtusifoliol 14α-methyl demethylase inhibitors†

Tom M Bargar, Jacob Secor, Lowell D Markley, Brian A Shaw and Jon A Erickson*

Dow AgroSciences, 9330 Zionsville Rd, Indianapolis, IN 46268, USA

Abstract: This report describes the development of a Comparative Molecular Field Analysis (CoMFA) model from a set of obtusifoliol 14α-methyl demethylase (DM) inhibitors to aid in the design of herbicides targeting sterol biosynthesis. CoMFA is a three-dimensional (3-D) quantitative structure–activity relationship (QSAR) method that is useful in the probing of receptor binding sites when experimental structure data are unavailable. Conformational analysis and SAR of some rigid and active analogs were used to build the initial model using the active analog hypothesis. The model was subsequently used to design compounds that retain the active site shape requirements, but incorporate physical properties that favor soil-applied herbicidal action. In addition, a second-generation CoMFA model incorporating the newly designed inhibitors was developed and represents the current understanding of the DM binding site. This model was derived from a pharmacophore developed from two methods, the active analog approach as well as from the Catalyst program. The fact that two independent methods produced a similar pharmacophore strengthens the validity of the model.

Keywords: comparative molecular field analysis; CoMFA; 3-D QSAR; pharmacophore; sterol biosynthesis; obtusifoliol 14α-methyl demethylase inhibitors; herbicide design

1 INTRODUCTION

Cytochrome-P450-dependent 14α-methyl demethylase (DM), an enzyme in the sterol biosynthesis pathway, converts lanosterol to ergosterol in fungi (cholesterol in mammals) and obtusifoliol to phytosterols (sitosterol, stigmasterol and campesterol) in plants.[1] Inhibitors of this pathway deprive organisms of important sterols needed for cell membranes, and thus are potential fungicides and herbicides. In fact, inhibitors of sterol biosynthesis (SBI) have been developed as commercial fungicides over the last twenty years.[2]

Many of the azole-type fungicides have been shown to inhibit obtusifoliol DM.[3,4] More recently, an indanyl-imidazole DM inhibitor, CGA201029 (**1;** Fig 1), has been demonstrated to have herbicidal activity.[5] Moreover, a number of analogs of 1 have been prepared providing a rudimentary structure–activity relationship (SAR) of the DM activity of this class.[6] In particular, the stereochemistry of C_1 of the indanyl ring is important since the (*R*)-isomer is greater than twenty times more active than the (*S*)-isomer.[6] Removing N_3 from the imidazole (the pyrrole analog) eliminated DM activity, demonstrating that an unhindered aromatic nitrogen is essential for binding to the enzyme. Elimination of the carbomethoxy group also reduced activity, the I_{50} value increasing from 30 nM to 155 nM, suggesting an important role for this substitutent.[6] Hydrolysis of the ester to the acid analog greatly reduced activity (by over fifty times) implying an intolerance for an acid functionality in this portion of the binding pocket.[6] Modifications of the indanyl portion of the molecule were tolerated and included halo substitution and replacement of the indane with tetralin, chromanone, and diaryl groups.[6] These substitutions suggest some flexibility in the hydrophobic portion of the binding pocket.[6] In fact, computer-aided superpositioning studies of the (*R*)- and (*S*)-isomers of **1** (five-membered) and the tetralin (six-membered) analogs have been used to suggest an active-site model that was useful in forecasting the inactivity of the corresponding four- and seven-membered ring analogs.[7]

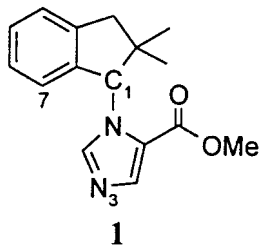

1

Figure 1. Structure of CGA201029.

* Correspondence to: Jon A Erickson, Eli Lilly and Co, Lilly Corporate Center, Indianapolis, IN 46285, USA
E-mail: jae@lilly.com
† Presented in part at the 215th National American Chemical Society Meeting, 29 March–2 April 1998, Dallas, TX, USA
(*Received 3 September 1998; revised version received 12 April 1999; accepted 30 June 1999*)

 Pestic Sci 0031–613X/99/$17.50

Although there has been only limited computational work in the obustifoliol DM inhibitor (herbicide) area, there are a number of studies involving the design of lanosterol DM inhibitors.[8] Many of these studies were prompted by spectral evidence that azole DM inhibitors bind to the heme group of the enzyme.[9,10] In general, these models consisted of the unhindered aromatic nitrogen bound to the heme group as an axial ligand with a hydrophobic cavity defined by an overlay of the various azole-type of DM inhibitors and often the substrate, lanosterol, with the 14α-methyl group above the heme iron.[11–15] These models were useful in understanding the activities of analogs within a class and in the design of further analogs.

Although experimental (X-ray or NMR) structures of lanosterol and obtusifoliol DM are not available, attempts to model the tertiary structure of DM have been reported. A homology model of lanosterol DM from *Saccharomyces cerevisiae* was constructed from the X-ray crystallographic structure of cytochrome P450 camphor 5-exo-hydroxylase from *Pseudomonas putida*, the only P450 class enzyme whose 3-D structure has been solved.[16] The model was used to explain experimental activity trends by docking known inhibitors.[16] Similarly, a DM homology model from *Candida albicans* was constructed from the *P putida* structure and was used to examine the binding of substrate.[17]

Design of enzyme inhibitors without the aid of an experimental structure of the inhibitor bound to the protein relies on the development of quantitative structure–activity relationships (QSAR). A powerful type of QSAR, known as 3-D QSAR, utilizes the three-dimensional geometry of inhibitors in order to develop a model of the enzyme binding pocket.[18] Knowing the shape and electronic features of the inhibitor binding pocket can aid in the design of novel and potent inhibitors. Comparative molecular field analysis (CoMFA) is a 3-D QSAR method that involves calculation of atomic interactions of analogs in a 3-D grid of points and using these potentials as the independent variables in a regression model.[19] This method has been applied to a class of azole antifungal agents for the purpose of further synthetic exploitation.[20] Here the CoMFA method is applied to a series of obtusifoliol DM inhibitors to assist in the direction of herbicide synthesis.

2 METHODS

2.1 Computational methods

In general, the basic steps involved in developing a CoMFA model are: (1) calculate 3-D structures and atomic charges of analogs in a chosen conformation; (2) overlay all molecules in a chosen alignment pattern; (3) place each molecule in a grid of points, calculate atom-to-point potentials for each and transfer the results into columns of a regression table; (4) use partial least squares (PLS) technique[21] to derive a regression model. The model can be used in a similar fashion to a traditional QSAR model for predictions, but has the added feature that allows the 3-D visualization of the response. The high and low values of the model can be mapped back onto the 3-D grid so that areas where atomic properties (steric and electronic) increase or decrease activity can be visualized. These maps can be used in place of a model of the enzyme binding pocket in an inhibitor design sense.

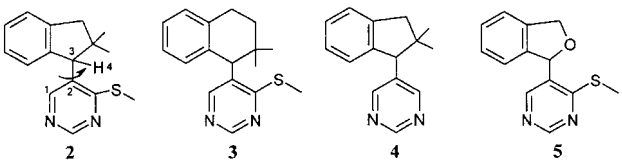

Figure 2. Structures of representative analogs used to define the active conformation.

In the CoMFA method two major issues must be addressed, namely the conformation and alignment of the training set of molecules. The binding conformation of each inhibitor is generally not known and only a single conformation can be selected for the CoMFA method. Selection of only one conformation can introduce significant bias into the model. In addition, all analogs must be aligned within the grid, with the pharmacophoric points in the same region of space;

Table 1. Obtusifoliol DM activity of the initial CoMFA training set

Molecule	prl_{50}[a]	*Molecule*	prl_{50}[a]
1	9.41	**30**	8.46
2	9.00	**31**	7.81
3	8.87	**32**	7.91
4	7.06	**33**	7.64
5	5.75	**34**	8.06
6	7.35	**35**	8.44
7	8.75	**36**	8.81
8	8.60	**37**	9.34
9	9.03	**38**	9.02
10	8.58	**39**	8.38
11	5.72	**40**	7.68
12	8.71	**41**	8.67
13	8.18	**42**	8.08
14	7.75	**43**	7.37
15	8.39	**44**	8.18
16	8.75	**45**	8.20
17	6.61	**46**	6.60
18	8.92	**47**	8.16
19	8.31	**48**	8.03
20	8.29	**49**	9.09
21	6.86	**50**	7.71
22	8.45	**51**	7.92
23	8.90	**52**	7.79
24	9.05	**53**	8.34
25	6.37	**54**	8.65
26	8.63	**55**	5.78
27	8.94	**56**	5.94
28	8.72	**57**	7.67
29	8.57	**58**	7.08

[a] $prl_{50} = \log(1/rl_{50})$.

again, this decision can introduce bias into the final model.

Due to the importance of conformation and alignment, some SAR and conformational analysis of representative classes of the inhibitors must first be carried out to find the key pharmacophoric points and common low-energy conformations. This approach is known as the active analog method.[22–24] To select a conformation to use in the CoMFA model, a few of the more active and rigid DM inhibitors were chosen for conformational analysis. In most of the analogs there is a heterocycle (pyrimidine, imidazole, triazole) bonded to a lipophilic backbone (indane, tetraline, dibenzosuberane, dibenzodioxicin). To determine the favored conformation about this bond, it was driven from 0 to 360° in 10° increments, allowing the rest of the molecule to relax at each point using MOPAC[25] with the AM1 Hamiltonian.[26] The molecules subjected to the conformational analysis and the definitions of the driven torsions (1-2-3-4) are shown in Figs 1 and 2. The stereoisomer corresponding to (*R*)-**1** was used.[6]

From the results of the conformational search, a common low-energy conformation was chosen (see Section 3) as a starting point for full minimization on the remaining 53 analogs in the initial training set (see Table 1 and Fig 1–3). Synthesis of these analogs has been described previously.[27] Molecular geometries and Mulliken charges were calculated using MOPAC/AM1 using the keywords: PREC MULLIK EF NODIIS. Since the CoMFA method requires only

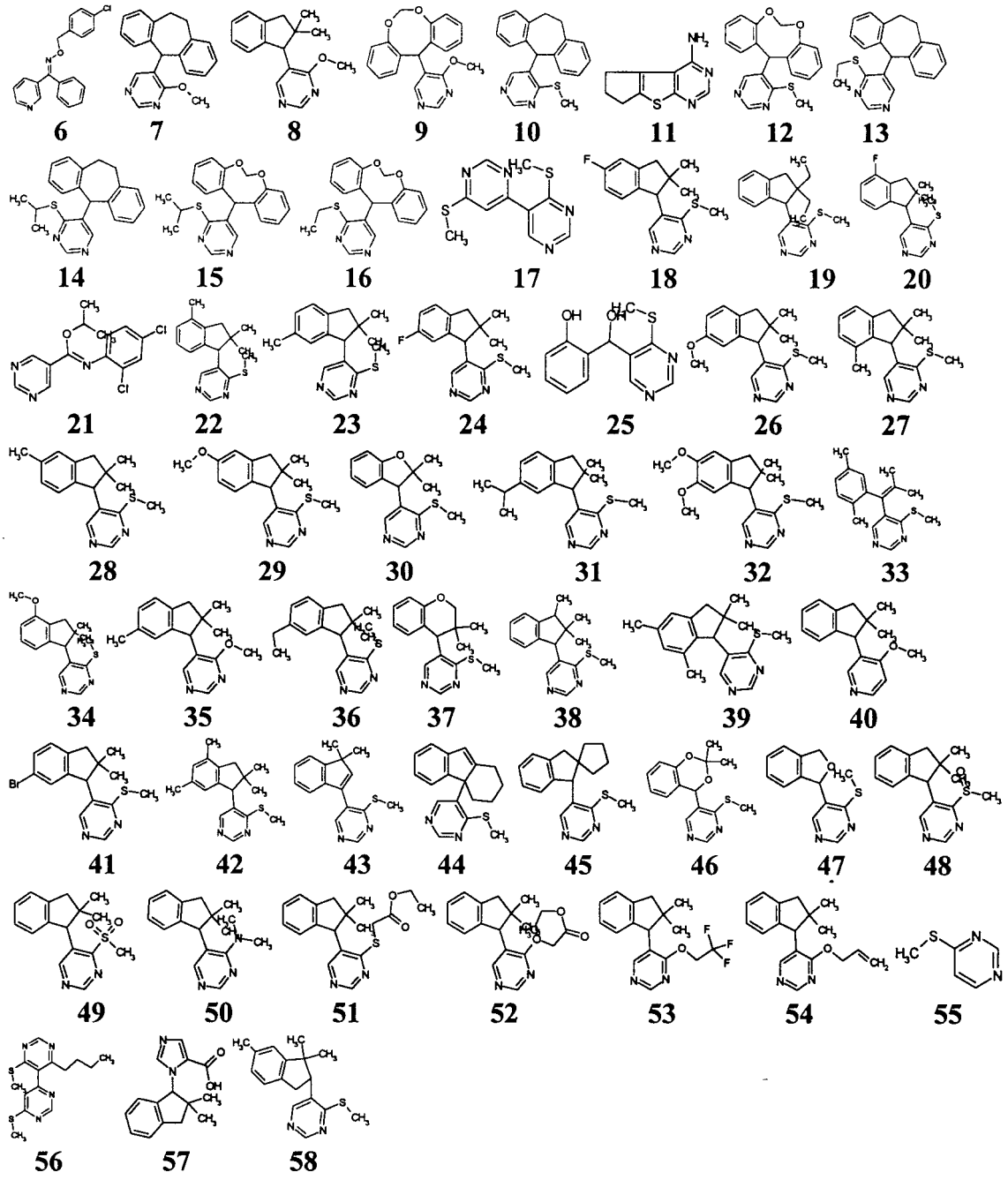

Figure 3. Structures of the initial CoMFA training set.

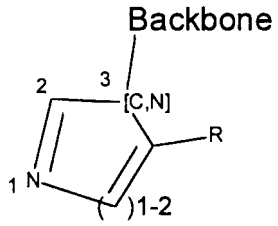

Figure 4. Generic structure of DM inhibitors.

similar low-energy structures, the MOPAC/AM1 geometries were not verified as minima by normal mode calculation. Molecular alignment within the CoMFA grid was based on the initial SAR already available.[6] Since all of the inhibitors have a nitrogen heterocycle that is believed to interact with the heme iron through their non-hindered aromatic nitrogen, all the molecules were aligned by an RMS fit of atoms 1, 2 and 3 as shown in Fig 4.

The molecular modeling program SYBYL (version 6.22)[28] was used to perform all CoMFA calculations. The CoMFA potential fields were determined by constructing a 3-D rectangular lattice (size based on the maximum extents of the molecules plus 4.0 Å) of points evenly spaced at 2.0 Å . An sp^3 carbon with a +1 point charge was placed at each grid point, and the resulting steric and electrostatic potentials for each molecule were calculated and placed in columns of the QSAR table for use as independent variables. The dependent variable was prI_{50} defined as: $\log(1/rI_{50})$ where rI_{50} (relative I_{50}) is the obtusifoliol DM inhibitor I_{50} (molar concentration at 50% inhibition) relative to compound 2 (see Fig 2), whose rI_{50} is defined as 1.0, but whose I_{50} is actually ~1.1 nM (see section 2.2). A fully cross-validated (leave-one-out protocol) PLS analysis was carried out in order to determine the predictive r^2 (also known as q^2) and the optimum number of components. This was followed by a PLS analysis with the optimum number of components to derive the predictive regression model. CoMFA coefficient maps and predictions are derived from this model.

A second-generation CoMFA model was also derived using a set of 45 DM inhibitors selected from over 350 compounds assayed since the derivation of the initial model (see Table 2). This training set was selected in order to maximize the diversity of backbones and heme binders within the available superset. The second generation CoMFA model was developed as described above.

In addition to the traditional active analog approach, a second, independent active conformation and pharmacophoric alignment derivation method was applied utilizing the program, Catalyst.[29–31] Catalyst employs a conformational sampling protocol in connection with a pattern recognition algorithm to identify a pharmacophore. The results include a hypothesis (or pharmacophore) consisting of up to five features (ie H-bond acceptors and donors, hydrophobes and charged groups) in a specific 3-D orientation. Catalyst also produces conformations and alignments of molecules in the training set that are useful as input for CoMFA. The second-generation CoMFA training set (Table 2) was also used in the Catalyst calculations. Each of the 45 molecules was subjected to conformer generation using the 'best quality' and a 20 kcal mol^{-1} energy range. A spreadsheet (Generate Hypothesis Workbench) was created and the rI_{50} entered for each compound with an uncertainty set to 3.0. The Exclude/OR Quicktool was used to create a new feature, an aromatic nitrogen H-bond acceptor for use in hypothesis generation. The hypothesis was generated using the known pharmacophoric features, 0 to 1 aromatic nitrogen H-bond acceptor and up to five hydrophobic groups. All of the default settings were used save the spacing (250), MinPoints (3) and MinSubsetPoints (2). The conformations and alignments were then used as direct input for CoMFA. Although the geometries created by Catalyst were used, Mulliken atomic charges were calculated with MOPAC for consistency with the initial and second-generation CoMFA models.

Table 2. Obtusifoliol DM activity of the second generation CoMFA training set[a]

Molecule	prl_{50}[b]	*Molecule*	prl_{50}[b]
1	9.52	**72**	6.92
2	9.00	**73**	5.92
3	8.87	**74**	6.60
4	7.06	**75**	6.88
5	5.75	**76**	7.89
9	9.11	**77**	7.84
10	8.61	**78**	4.99
37	8.85	**79**	4.98
40	7.68	**80**	8.14
58	7.08	**81**	9.01
59	7.83	**82**	7.42
60	7.13	**83**	9.22
61	7.99	**84**	8.19
62	8.43	**85**	7.25
63	5.64	**86**	7.21
64	8.56	**87**	8.31
65	6.93	**88**	8.48
66	6.22	**89**	9.06
67	6.96	**90**	8.48
68	7.25	**91**	8.13
69	7.61	**92**	8.71
70	7.66	**93**	8.84
71	8.07		

[a] This table has 10 molecules in common with Table 1; however, prI_{50} values differ slightly for **1**, **9**, **10**, and **37**. The discrepancy arose where compounds were re-tested after derivation of the initial model. Because some compounds were assayed multiple times, average values were used.
[b] $prI_{50} = \log(1/rI_{50})$.

2.2 Biological activity

In each test there were three control vials and two

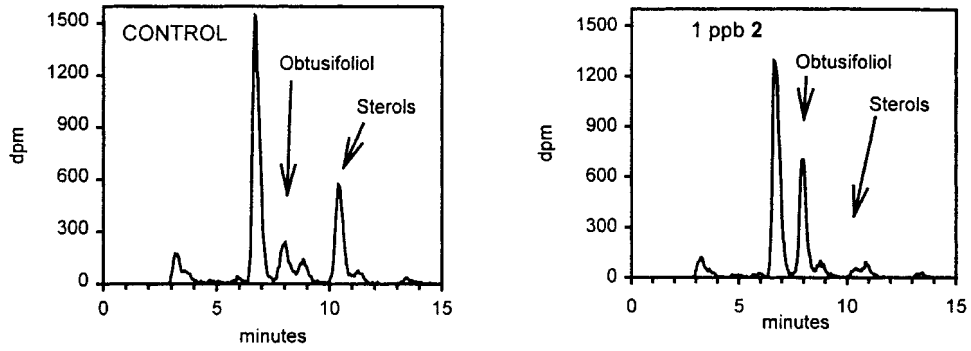

Figure 5. Radiochromatograms of nonsaponifiable lipids extracted from control and **2**-treated barnyardgrass leaf pieces incubated in [1-^{14}C] acetate.

replications of each compound treatment. Compounds were tested at two concentrations, which were tenfold different. I_{50} values were calculated based on the formula:

$$I_{50} = \frac{\text{inhibitor concentration} \times (100 - \%\ \text{inhibition})}{\%\ \text{inhibition}}$$

for each of the four values per compound (two replicates at two concentrations).[32] This formula yields an accurate estimate for I_{50} only when inhibition is between 10 and 90%, thus, only data within this range were used in the calculation. In each set of assays, an internal standard, **2**, was included and the data were expressed as a relative I_{50} (rI_{50}), which was calculated by dividing the I_{50} of the compound by the I_{50} of **2** in that test. The average I_{50} of **2** was 0.29 μg litre^{-1} (1.1 nM) for 103 sets of tests (standard estimate of the mean was 0.03 μg litre^{-1} and the standard deviation was 0.14 μg litre^{-1}).

Young (less than three-leaf stage) barnyardgrass (*Echinochloa crus-galli*) plants grown in soil in the greenhouse were harvested at the soil surface and small (2 to 3 mm) sections were cut acropetally from the stem to the second leaf collar and dropped into a 125-ml filter flask containing about 75 ml of water. The plant pieces were vacuum infiltrated by applying and releasing vacuum until they no longer floated. During this process the deionized water in the flask was changed three times with a total volume of 75 ml. After the final vacuum cycle, most of the water in the flask was decanted.

Approximately 1.0 g (±10%) of leaf pieces was transferred to a tared 20-ml glass scintillation vial and then 5 ml water was added, followed by 50 μl of compound in acetone and 10 μl [1-^{14}C]acetate (2 μCi, 60 μCi μmol^{-1}). The final concentration of acetone was 10 ml litre^{-1} in both test and control vials. The rack of vials was covered with Saran® plastic film and incubated at 30 °C for 16 h in light. It was verified that the system was in equilibrium at 16 h. The light source was a 300-W quartz halogen lamp suspended approximately 50 cm above the vial rack, providing saturating illumination for photosynthesis.

At the end of the incubation period, the bathing solution was discarded and the tissue was extracted and saponified with the addition of methanolic potassium hydroxide (150 g litre^{-1}, 3 ml). The vials were tightly capped with Teflon-lined lids and placed in a rapidly shaking water bath at 70 °C for no less than 60 min. At the conclusion of the saponification period, the vials were cooled to room temperature and the sterols were extracted by washing the potassium hydroxide/methanol solution with hexane (3 × 5 ml). The hexane extracts were pooled and dried under nitrogen. The dried hexane fractions were then solubilized in 250 μl hexane and passed through 0.2-μm nylon filters into 4-ml autosampler vials.

Sterol analysis was performed using a normal-phase HPLC system consisting of an Altech Altima Silica column (Cat No 88172, 250 × 4.6 mm). A 125-μl sample was injected onto the column and the chromatography was accomplished isocratically at a flow rate of 1 ml min^{-1} using hexane + 2-propanol (98.5 + 1.5 by volume). Absorbance was monitored at 215 nm and radioactivity was monitored using an INUS Betaram detection system. The areas under the obtusifoliol and sterol peaks were integrated and expressed as a percentage of dpm injected. Typical radiochromatograms are shown in Fig 5. Final sterols including stigmasterol, sitosterol, and campesterol elute as a single peak at about 10.5 min. Obtusifoliol, the substrate for the demethylase, elutes at about 8 min. The inhibition of the demethylase results in a decrease in the final sterol peak with a concomitant increase in the obtusifoliol peak. Racemic mixtures of all chiral compounds were assayed.

3 RESULTS AND DISCUSSION

3.1 Initial CoMFA model

The conformation selected for the initial CoMFA model was based on the conformational analysis of the compounds **1, 2, 3, 4**, and **5** (Figs 1 and 2) using MOPAC as described in the Section 2.1. The results of the grid searches are shown in Fig 6. In each case, the relative AM1 heat of formation (H_f - H_f (lowest energy conformer)) is plotted versus the torsion angle as defined in Fig 2. Compound **2** was chosen as the 'active analog' because of its high activity and its rigid

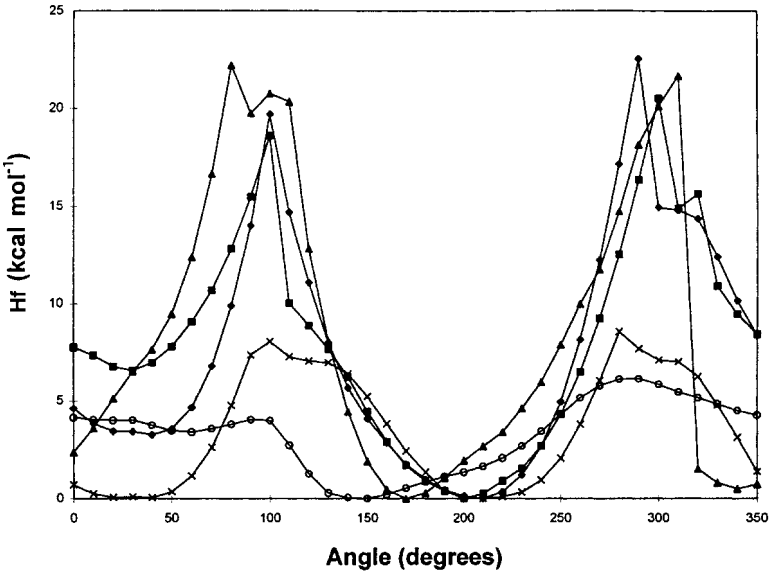

Figure 6. MOPAC/AM1 conformational grid plot of compounds (■) **1**, (◆) **2**, (▲) **3**, (×) **4** and (○) **5**.

structure. Figure 6 shows that it has two minima, one at 30° which lies about 3 kcal mol^{-1} above the other minimum at 220°. The minimum at 220° was chosen to be the conformation used in the CoMFA analysis because it is also the minimum of two other very active analogs, **1** and **3** (see Fig 6) which represent changes in the backbone and heterocycle portions of the class. Besides the energetic advantage of this conformation, the restricted rotation about the scanned bond (~18 kcal mol^{-1} for **1, 2** and **3**) seems to impart greater activity, presumably due to entropy. Two analogs, **4** and **5**, which have much smaller barriers, 8 and 4 kcal mol^{-1}, respectively (see Fig 6), bind weakly to the enzyme (see Table 1).

A set of 58 compounds for which obtusifoliol DM I_{50} values were available was chosen as the initial CoMFA training set. Their structures are shown in Figs 1, 2 and 3 and their prI_{50} values in Table 1. The results of the crossvalidated-PLS and PLS analyses are given in Table 3. The actual versus predicted plot of the initial CoMFA model is shown in Fig 7. The steric and electrostatic CoMFA coefficient maps are shown in plate 1. The steric contours consisted of the standard deviation*coefficient mapped at the 70% contribution level for the high values (ie contours where steric bulk increases activity) and 30% contribution for the low values (ie contours where steric bulk decreases activity). The electrostatic contours

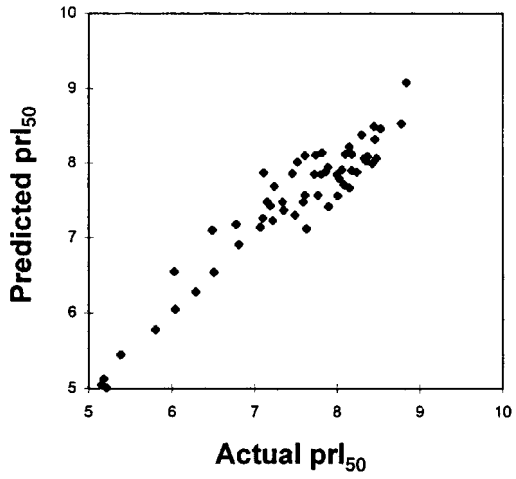

Figure 7. Actual versus predicted plot for the initial CoMFA model.

Table 3. Results of the PLS analyses for each training set and alignment method

	Initial training set: active analog	*2nd generation training set: active analog*	*2nd generation training set: catalyst*
Cross-validated (leave-one-out):			
No of observations	58	45	45
Optimal no of components	4	4	2
q^2	0.634	0.587	0.270
Standard error of predictions	0.583	0.761	0.988
PLS at optimal no of components:			
Standard error of estimate	0.307	0.342	0.517
r^2	0.898	0.917	0.800
F value	116.744	110.114	84.074
Probability $r^2=0$	0.0	0.0	0.0

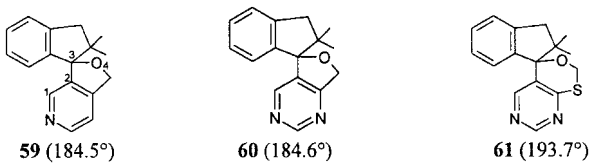

Figure 8. Structures of conformationally restricted analogs. (MOPAC/AM1 minimum 1-2-3-4 torsion angles in parentheses.).

Figure 9. Lipophilic design lead and its des-SMe analog.

were mapped at 80% contribution level for the high values (ie contours where positive charge increases activity) and 20% contribution for the low values (ie contours where positive charge decreases activity). The steric map (Plate 1A) reveals that there is a concave contour about the indanyl ring representing an area where steric bulk decreases activity and may be thought of as the sides of the binding pocket for which the indanyl ring of **1** seems ideally shaped. Another edge of the pocket may be modeled by the yellow contours about the *ortho*-imidazole position, suggesting that large substituents in this area may decrease binding affinity. There is a green region close to the 7-position of the indanyl ring (see Fig 1) reflecting the advantage of substitution in this position. There is also a sterically preferred region about the gem-dimethyl of the indane, suggesting the ability of the pocket to accommodate larger groups. The electrostatic map (Plate 1B) is dominated by blue regions indicating that partial positively charged or neutral groups are preferred in the binding pocket, although there is a dearth of partial negatively charged backbones in the training set.

3.2 Inhibitor design

The results of the initial CoMFA model and putative active conformation were used to design new ligands. Because the conformational analysis suggests that conformational restriction yields more potent DM inhibitors, analogs with locked conformations were examined. In addition to the conformational results reported here, the activity of compound **59** (Fig 8) also suggested that a restricted conformation may increase enzyme affinity. Its I_{50} relative to **2** was 15, making it slightly more efficacious than the analogous *ortho*-methoxy pyridine analog, **40**, ($rI_{50}=21$) with a predicted rI_{50} from the CoMFA model of 41. Since a restricted conformation combined with the more potent pyrimidine ring may increase enzyme affinity, molecules **60** and **61** were proposed as synthetically obtainable targets. The predicted rI_{50} values for **60** and **61** were 57 and 22, respectively. Any entropic gain in binding affinity, however, would not be reflected in the CoMFA prediction. The actual rI_{50} values revealed (**60** = 75 and **61** = 10) that the restricted conformations did not increase binding and were fairly close to their predicted values. Insight into the activity of these analogs may be gained by examination of the grid searches of the highly active analogs (see Fig 6) which reveal energy wells that are fairly broad (~70°) suggesting that some flexibility may be needed to achieve the optimal binding conformation. The higher activity of **61** over **60** may be explained by its increased flexibility and/or that its minimum torsion angle lies closer to the ideal (~220°). In addition, the fact that the CoMFA predictions were close may suggest that these spiro-substitutents are not optimal.

Another area of design involved the introduction of polar groups into this class of DM inhibitor in an attempt to improve physical properties needed for soil-applied herbicidal action (ie lower lipophilicity). From the CoMFA model (see Plate 1) it was apparent that larger groups would be allowed in the regions about the gem dimethyl of the indanyl group (green contours). All of the groups in this area of space in the training set were relatively non-polar, so in order to explore the tolerance of polar groups some additional analogs were needed. As a template, the fairly active but lipophilic analog, **62** ($rI_{50}=4$; ClogP = 4.04)[33] shown in Fig 9, was chosen. A conformational search similar to those described above was carried out, revealing a similar profile (Fig 10) to the highly active analogs: a minimum at ~150° with a relatively high barrier to rotation. This conformer (150° minimum) overlays well with the minimum of **2** used in the CoMFA model. In fact, the grid search (Fig 10) of the much weaker des-SMe analog (**63**, $rI_{50}=2291$; see Fig 10) shows a lower barrier to rotation (~1 vs ~4 kcal mol^{-1} for **62**).

Two general templates (see Fig 11) were selected to mimic the shape of the bisphenyl pyrimidine (**62**) with polar groups, and for synthetic accessibility. Conformational searches were carried out for each of the templates for comparison to the known active analogs. Figure 12 shows that the two molecules have a very similar conformational profile to that of **62**. Placing the minimum energy conformation of each in the CoMFA coefficient maps shows a very good fit, especially for the sulfonamide analog (Plate 2) which tends to fill in the favored regions about the indanyl gem-dimethyl very nicely. The imidazole is too small to fill in this region, which is reflected in the predicted rI_{50} values for the two templates: template 1 = 34 and 2 = 96. It should be noted that there was a high degree of extrapolation in these predictions due to the lack of polar functionality in this region of space in the training set. In addition, the predicted rI_{50} for **62**, which was not in the training set, was considerably higher than the actual value (predicted $rI_{50}=125$). Since these templates were consistent with the overall shape of the current pharmacophore, some analogs of

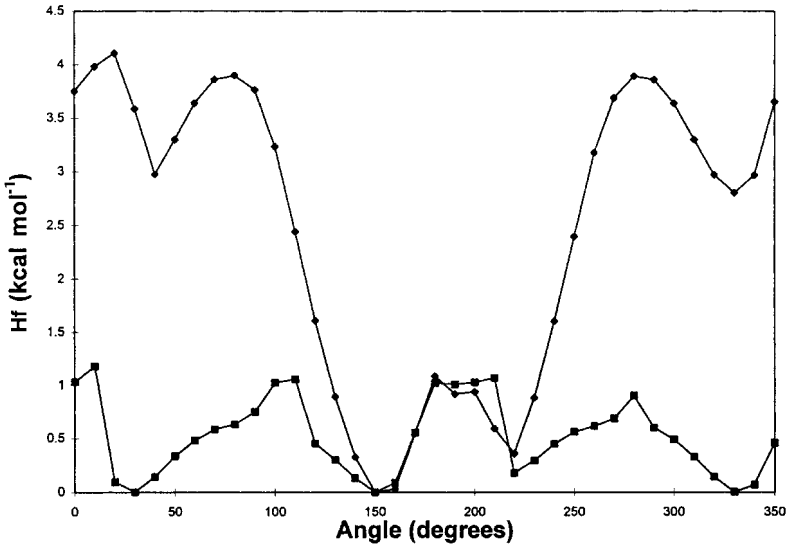

Figure 10. MOPAC/AM1 conformational grid plot of (◆) **62** and (■) **63**.

Figure 11. Structures of CoMFA designed DM inhibitors (ClogP values in parentheses[33]).

each were synthesized and tested against obtusifoliol DM. Template 1 (**64**) was measured to have $rI_{50}=3$, much better than the predicted value, demonstrating the tolerance for polar groups in this part of the pocket. Template 2 was not synthesized, but an analog, **65**, had $rI_{50}=117$, again indicating that polarity is tolerated but the shape of the imidazole is not quite ideal for binding, as indicated by the CoMFA model. Using the CoMFA model to guide the shape of newly designed analogs allowed an increase in polarity (lowered ClogP by ~3 units) of the compounds that is needed for a soil-applied herbicide while retaining good affinity to the enzyme.

3.3 Second-generation CoMFA model

In addition to the initial CoMFA model described above, a second-generation model was derived in order to include some of the diverse chemistry synthesized and assayed since the initial training set was compiled. From a set of over 350 compounds for which DM inhibition data existed, a subset of 45 compounds was selected to represent the major changes in the backbone and heme binder. The activities of these compounds are listed in Table 2 and their structures are shown in Figs 8, 9 and Fig 13.

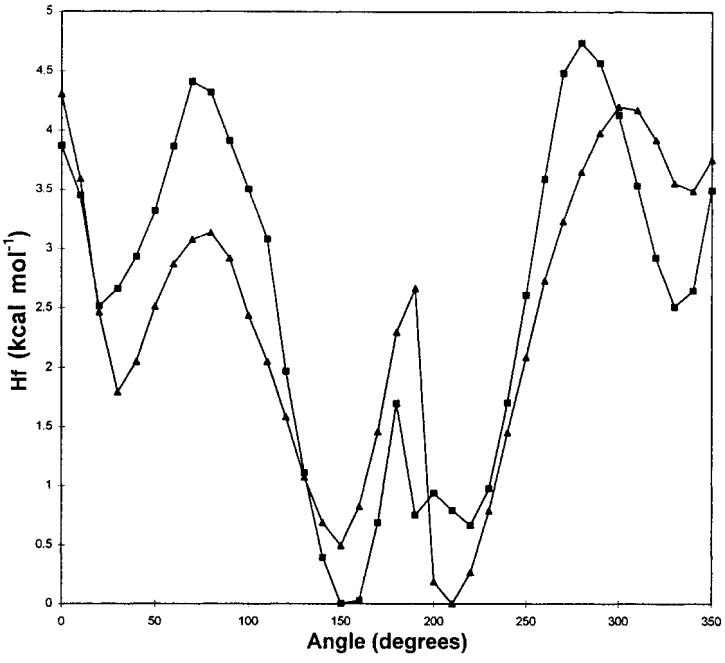

Figure 12. MOPAC/AM1 conformational grid plot of (▲) Template 1 and (■) Template 2.

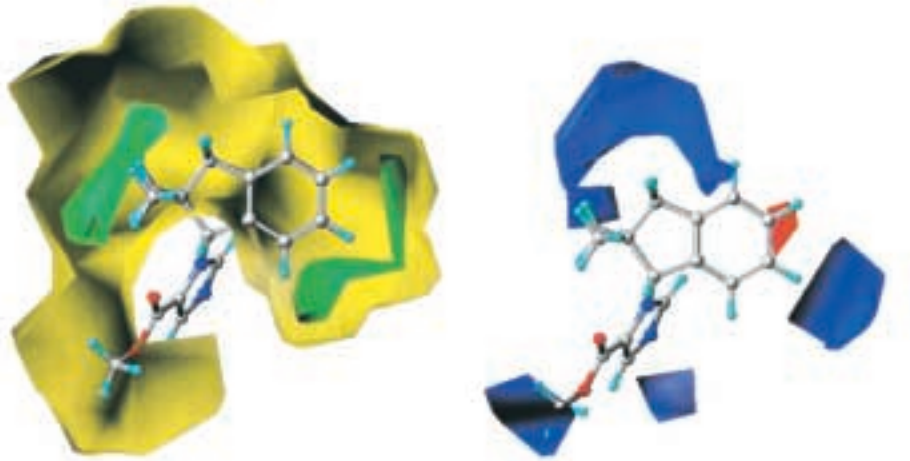

A. Steric Map **B.** Electrostatic Map

Plate 1. Steric and electrostatic initial CoMFA model coefficient maps with **1** (green = 70% contribution level; yellow = 30% contribution level; blue = 80% contribution level; red = 20% contribution level). The steric map is z-clipped (ie contours obscuring the structure are removed) to show the idanyl group.

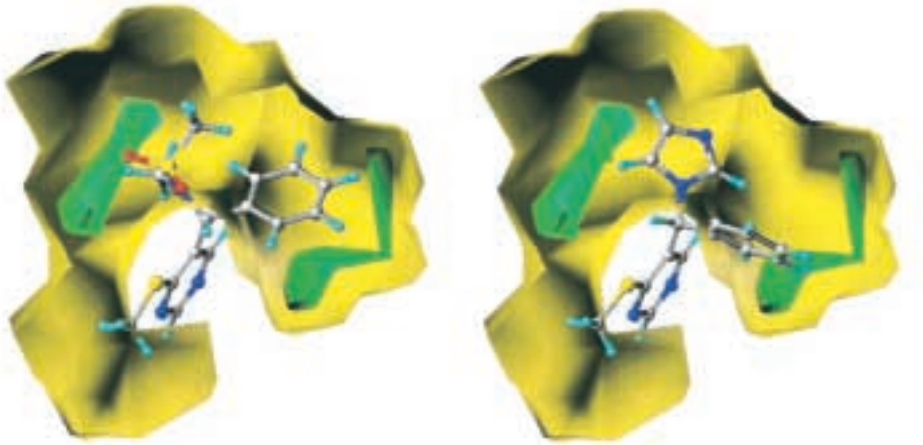

Template 1 Template 2

Plate 2. Steric initial CoMFA model coefficient map with templates 1 and 2 (green = 70% contribution level; yellow = 30% contribution level). The steric map is z-clipped to show the new backbone groups.

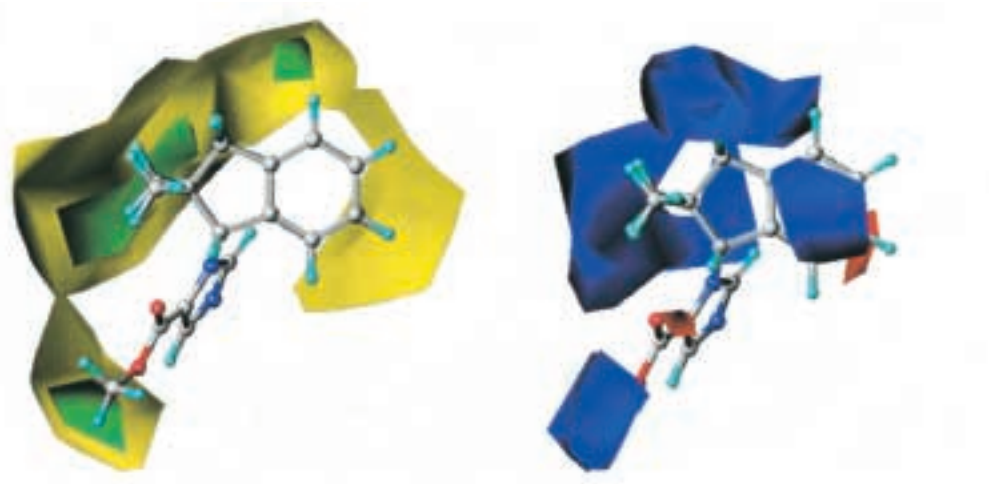

A. Steric Map **B.** Electrostatic Map

Plate 3. Steric and electrostatic second-generation CoMFA model coefficient maps with molecule **1** (green = 70% contribution level; yellow = 30% contribution level; blue = 80% contribution level; red = 20% contribution level). The steric map is z-clipped to show the idanyl group.

View 1 View 2

Plate 4. Catalyst hypothesis with the best conformer of **1**. (H-bond acceptor in red and three hydrophobes in green.)

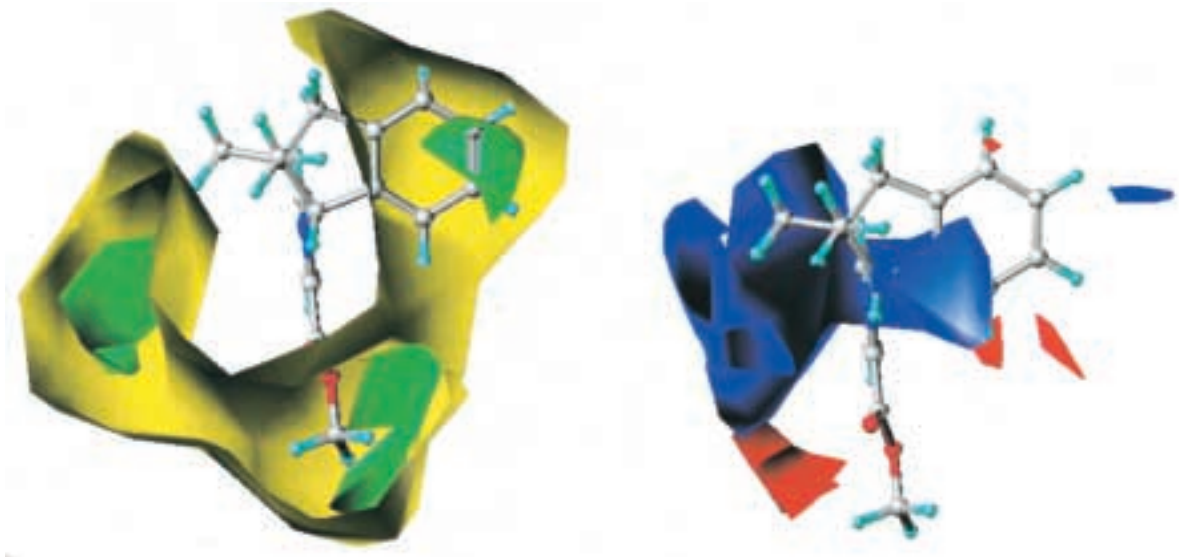

A. Steric Map **B.** Electrostatic Map

Plate 5. Steric and electrostatic catalyst CoMFA model coefficient maps with molecule **1** (green = 70% contribution level; yellow = 30% contribution level; blue = 80% contribution level; red = 20% contribution level). The steric map is z-clipped to show the idanyl group.

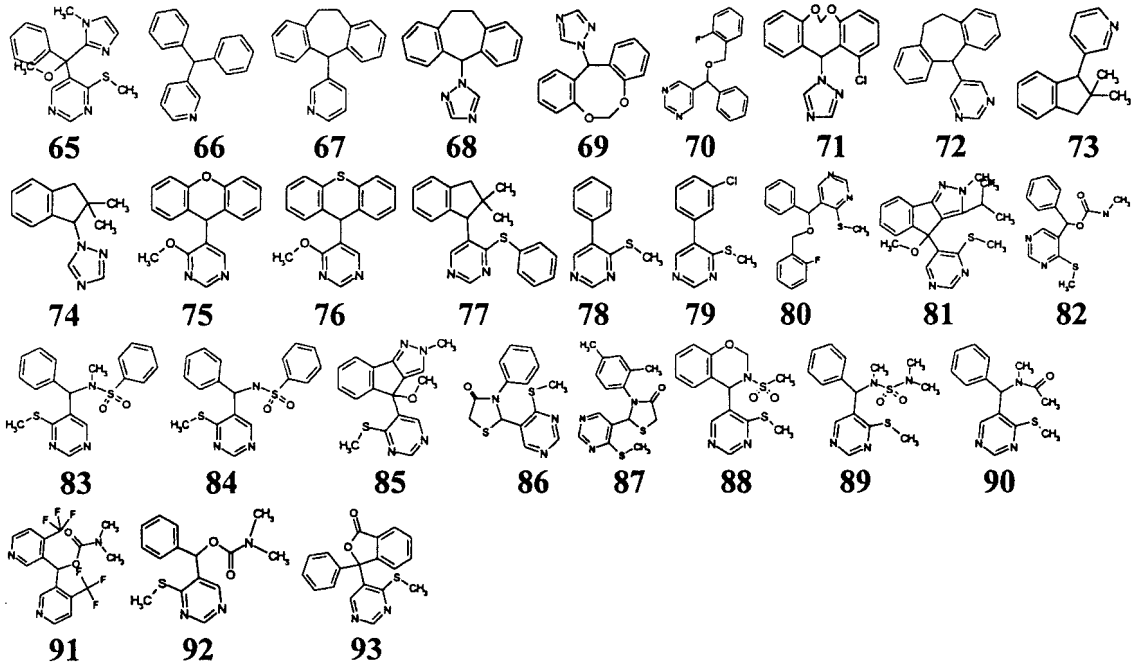

Figure 13. Structures of the second-generation CoMFA training set.

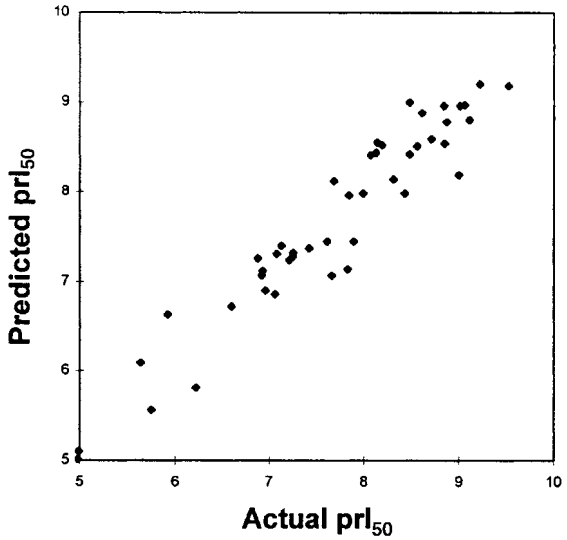

Figure 14. Actual versus predicted plot for the second-generation CoMFA model.

The results of the crossvalidated-PLS and PLS analyses are shown in Table 3. The actual versus predicted plot of the second CoMFA model is shown in Fig 14 and the CoMFA coefficient maps are displayed in Plate 3. Comparing the new model with the initial reveals that they are very similar with respect to the coefficient maps. Both have a similar shaped 'pocket' with favored steric responses in an area about the gem-dimethyl groups of the indane. The second-generation model has a sterically favored region in the vicinity of the carboxymethyl group, not present in the initial model. In addition, the second-generation model lacks the green (sterically favorable) region about the phenyl portion of the indane. These subtle differences in the two models reflect the lack of some of the substituted indanes in the second-generation training set. The electrostatic maps are also very similar to the original, despite the addition of many molecules with increased polarity to the training set. The region about the indanyl portions is larger reflecting greater change, but the model still prefers partial positively charged or neutral groups in this region over partial negatively charged groups.

3.4 Catalyst model

The results of the Catalyst model agree very well with the CoMFA and conformational work. The best hypothesis generated consisted of one aromatic nitrogen H-bond acceptor and three hydrophobic groups. The hypothesis is shown in Plate 4. The H-bond acceptor is centered on the unhindered aromatic nitrogen (see Plate 4, View 1,) in all cases, even for the pyrimidines and triazoles, which have two aromatic nitrogens. The best conformations for most of the compounds were very similar to those chosen from conformational analysis, although they did differ slightly with respect to rotation about the backbone-heme binder bond. This is not too surprising in the light of the broad minimum that was found to exist for this class. The hypothesis also contains three hydrophobic features centered on the indanyl group and the carbomethoxy on the imidazole (see Plate 4, View 2). These are areas where the CoMFA model predicted increased steric bulk to increase activity.

A final CoMFA model was derived using the conformations and alignments produced by Catalyst. The results of the crossvalidated-PLS and PLS analyses are shown in Table 3. The actual versus predicted plot of the catalyst-derived CoMFA model is shown in Fig 15. The statistics are not as robust as in the active-analog-derived model, but this is to be expected due to the

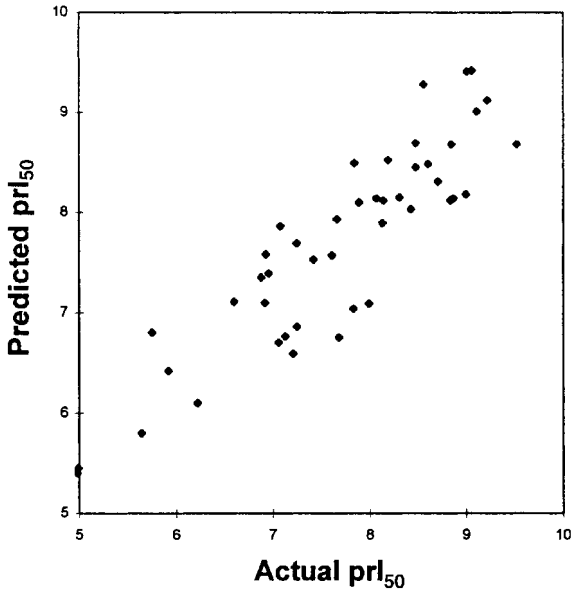

Figure 15. Actual versus predicted plot for the Catalyst CoMFA model.

coarseness of the Catalyst model. Several groups have, however, shown a q^2 of ~0.3 to be significant.[34,35] The CoMFA coefficient maps are shown in Plate 5. In general, the maps are very similar to the second-generation CoMFA model. In particular, the 'pocket' defined by the sterically disfavored regions is about the same shape as the previous model. It does differ slightly, which is an effect of the difference in backbone-heme binder torsion angle used in the two models. The CoMFA model again reflects the position of the three hydrophobes with sterically favored regions. The electrostatic map is very similar to the second-generation CoMFA, again dominated by blue regions about the backbone of the DM inhibitors.

4 CONCLUSION

The herbicide target, obtusifoliol 14α-methyl-demethylase, was probed by assaying a set of structurally diverse inhibitors. This effort refined the current models[6,7] describing the shape of the obtusifoliol DM binding pocket. The active-analog approach was utilized to propose an active conformation of various azole DM inhibitors leading to the development of a CoMFA model. This model was used to summarize what was known about the shape of the obtusifoliol DM inhibitor binding pocket and pointed to areas where synthetic modification would expand the SAR, further defining the attributes of the pocket. Specifically, some conformationally restricted analogs supported the active conformation selection, suggesting a hypothesis that both some backbone-heme binder flexibility and an *ortho*-substituent on the heme binder are important for activity. The initial CoMFA model was also useful in the design of some polar backbones. Conformational analysis combined with the CoMFA model accurately predicted the binding of some sulfonamide and imidazole backbone replacements. A second-generation CoMFA model that incorporated many of these newly designed analogs was subsequently developed to summarize the current SAR on the obtusifoliol DM binding pocket. The validity of this model was supported by the development of an additional CoMFA model based on the conformations and alignments from an independent pharmacophore generation method, Catalyst.

REFERENCES

1 Grunwald C, Plant sterols. *Annu Rev Plant Physiol* **26**:209–236 (1975).
2 Mercer EI, Sterol biosynthesis inhibitors: their current status and modes of action. *Lipids* **26**:584–597 (1991).
3 Rahier A and Taton M, The 14α-demethylation of obtusifoliol by a cytochrome P-450 monooxygenase from higher plants microsomes. *Biochem Biophys Res Commun* **140**:1064–1072 (1986).
4 Taton M, Ullmann P, Benveniste P and Rahier A, Interaction of triazole fungicides and plant growth regulators with microsomal cytochrome P-450-dependent obtusifoliol 14α-methyl demethylase. *Pestic Biochem Physiol* **30**:178–189 (1988).
5 Streit L, Moreau M, Gaudin J, Ebert E and Vanden Bossche H, A novel imidazolecarboxylic acid ester is a herbicide inhibiting 14α-methyl-demethylation in plant sterol biosynthesis. *Pestic Biochem Physiol* **40**:162–168 (1991).
6 Salmon F, Taton M, Benveniste P and Rahier A, Plant sterol biosynthesis: novel potent and selective inhibitors of cytochrome P450-dependent obtusifoliol 14α-methyl demethylase. *Arch Biochem Biophys* **297**:123–131 (1992).
7 Ramos TGM and Bellus D, Chirality and plant protection. *Angew Chem Int Edn Engl* **30**:1193–1215 (1991).
8 For a review see: Marriot MS, The rational design of fungal lanosterol C14 demethylase inhibitors, in *Molecular Aspects of Chemotherapy, Proc Int Symp*, 2nd edn, ed. by Borowski E and Shugar D, Pergamon, New York, NY. pp 193–204 (1990).
9 Yoshida Y and Aoyama Y, Interaction of azole fungicides with yeast cytochrome P-450 which catalyzes lanosterol 14α-demethylation, in *In-vitro and In-vivo Evaluation of Antifungal Agents*, ed by Iwata K and Vanden Bossche H, Elsevier, Amsterdam, Netherlands. pp 123–134 (1986).
10 Yoshida Y and Aoyama Y, Interaction of azole antifungal agents with cytochrome P-450 14DM purified from *Saccharomyces cerevisiae* microsomes. *Biochem Pharmacol* **36**:229–235 (1987).
11 Baldwin BC, Wiggins TE, Marchington AF and Worthington PA, The discovery and mode of action of PP450, a new broad-spectrum fungicide for cereals. *Meded Fac Landbouwwet Rijksuniv Gent* **49**:303–310 (1984).
12 Boyle FT, Gilman DJ, Gravestock MB and Wardleworth JM, Synthesis and structure–activity relationships of a novel antifungal agent, ICI 195,739. *Ann N Y Acad Sci* **544**:86–100 (1988).
13 Nakayama A, Ikura K, Katsuura K, Hashimoto S and Nakata A, Quantitative structure–activity relationships, conformational analyses, and computer graphics study of triflumizole analogs, fungicidal *N*-(1-imidazol-1-ylalkylidene)anilines. *Nippon Noyaku Gakkaishi (J Pestic Sci)*, **14**:23–37 (1989).
14 Lewis DFV, Rodrigues AD, Ioannides C and Parke DV, Adverse reactions of imidazole antifungal agents: computer graphic studies of cytochrome P-450 interactions. *J Biochem Toxicol* **4**:231–234 (1989).
15 Reynolds CH and Shaber SH, Rational design of novel ergosterol biosynthesis inhibitor fungicides, in *Computer-Aided Molecular Design, ACS Symposium Series* No 589 American Chemical Society, Washington DC. pp 171–182, 2 Plates - pp 230a–230b (1995).
16 Morris GM and Richards WG, Molecular Modeling of the sterol C-14 demethylase of *Saccharomyces cerevisiae*. *Biochem Soc Trans.* **19**:793–795 (1991).

17 Boscott PE and Grant GH, Modeling cytochrome P450 14α demethylase (*Candida albicans*) from P450cam. *J Mol Graphics* **12**:185–192 (1994).
18 For a review see: *3D QSAR in Drug Design*, ed by Kubinyi H, ESCOM, Leiden, The Netherlands (1993).
19 Cramer RD III, Patterson DE and Bunce JD, Comparative molecular field analysis (CoMFA). 1. Effect of shape on binding of steroids to carrier proteins. *J Am Chem Soc* **110**:5959–5967 (1988).
20 Tafi A, Anastassopoulou J, Theophanides T, Botta M, Corelli F, Massa S, Artico M, Costi R, Di Santo R and Ragno R, Molecular modeling of azole antifungal agents active against *Candida albicans*. 1. A comparative molecular field analysis study. *J Med Chem* **39**:1227–1235 (1996).
21 Lindberg W, Persson J-A and Wold S, Partial least-squares method for spectrofluorimetric analysis of mixtures of humic acid and lignin sulfonate. *Anal Chem* **55**:643–648 (1983).
22 Marshall GR, Barry CD, Bosshard HE, Dammkoehler RA and Dunn DA, The conformational parameter in drug design The active analog approach, in *Computer-Assisted Drug Design*, *ACS Symp. Series* No **112** (*Computer-Assisted Drug Des.*) ed by Olson EC and Christoffersen RE, American Chemical Society, Washington, DC. pp 205–226 (1979).
23 Mayer D, Naylor CB, Motoc I and Marshall GR, A unique geometry of the active site of angiotensin-converting enzyme consistent with structure–activity studies. *J Comput - Aided Mol Des.* **1**:3–16 (1987).
24 Dammkoehler RA, Karasek SF, Shands EFB and Marshall GR, Constrained search of conformational hyperspace. *J Comput - Aided Mol Des* **3**:3–21 (1989).
25 Stewart JJP, *MOPAC93*, Fujitsu Ltd. Tokyo, Japan (1993).
26 Dewar MJS, Zoebisch EG, Healy EF and Stewart JJP, Development and use of quantum mechanical molecular models. 76. AM1: a new general purpose quantum mechanical molecular model. *J Am Chem Soc.* **107**:3902–3909 (1985).
27 Markley LD, Ray PG, Arndt KE, Balko TW, Cressman ENK, Jackson JL, Ouse DG and Secor J, Preparation of 4-substituted 5-polycyclylpyrimidine herbicides. Int Patent Appl, 1997.
28 *SYBYL 6.22*, Tripos Inc, St Louis MO (1996).
29 *Catalyst Tutorials Release 3.0* (1996).
30 Barnum D, Greene J, Smellie A and Sprague P, Identification of common functional configurations among molecules. *J Chem Inf Comput Sci* **36**:563–571 (1996).
31 Smellie A, Teig SL and Towbin P, Poling: promoting conformational variation. *J Comput Chem* **16**:171–187 (1995).
32 Job D, Cochet C, Dhien A and Chambaz EM, A rapid method for screening inhibitor effects: determination of I_{50} and its standard deviation. *Anal Biochem* **84**:68–77 (1978).
33 *CLOGP:* BioByte Corp, Claremont, CA, USA.
34 Clark M, Cramer RD III, Jones DM, Patterson DE and Simeroth PE, Comparative molecular field analysis (CoMFA). 2. Toward its use with 3D-structural databases. *Tetrahedron Comput Methodol* **3**:47–59 (1990).
35 Thomas BF, Compton DR, Martin BR and Semus SF, Modeling the cannabinoid receptor: a three-dimensional quantitative structure–activity analysis. *Mol Pharmacol* **40**:656–665 (1991).